

A HIGH ORDER POSITIVITY PRESERVING DG METHOD FOR COAGULATION-FRAGMENTATION EQUATIONS

HAILIANG LIU*, ROBIN GRÖPLER**, AND GERALD WARNECKE**

ABSTRACT. We design, analyze and numerically validate a novel discontinuous Galerkin method for solving the coagulation-fragmentation equations. The DG discretization is applied to the conservative form of the model, with flux terms evaluated by Gaussian quadrature with $Q = k+1$ quadrature points for polynomials of degree k . The positivity of the numerical solution is enforced through a simple scaling limiter based on positive cell averages. The positivity of cell averages is propagated by the time discretization provided a proper time step restriction is imposed.

Key words. population balance equation, aggregation, breakage, discontinuous Galerkin method, conservation law, particle systems, high order accuracy

AMS subject classifications. 65M60, 65M12, 65R20, 35L65, 82C22

1. INTRODUCTION

The aggregation-breakage population balance equations (PBEs) are the models for the growth of particles by combined effect of aggregation and breakage. These equations are a type of partial integro-differential equations which are also known as coagulation-fragmentation equations. These models describe the dynamics of particle growth and the time evolution of a system of particles under the combined effect of aggregation, or coagulation, and breakage, or fragmentation. Each particle is identified by its size, or volume, which is assumed to be a positive real number. From a physical point of view the basic mechanisms taken into account are the coalescence of two particles to form a larger one and the breakage of particles into smaller ones. These models are of substantial interest in many areas of science and engineering.

The equations we consider in this paper describe the time evolution of the particle size distribution (PSD) under the simultaneous effect of binary aggregation and multiple breakage. The objective of this work is to design a high order discontinuous Galerkin method for these equations, so that the numerical solution is highly accurate, and remains non-negative.

In 1917, Smoluchowski [27] proposed the discrete aggregation model in order to describe the coagulation of colloids moving according to a Brownian motion which is known as Smoluchowski coagulation equation. In 1928, Müller [22] provided the continuous version of this equation as

$$\partial_t f(t, x) = \frac{1}{2} \int_0^x K(x-y, y) f(t, x-y) f(t, y) dy - \int_0^\infty K(x, y) f(t, x) f(t, y) dy$$

with

$$f(0, x) = f_0(x).$$

Date: October 2, 2017.

*Mathematics Department, Iowa State University, Ames, IA 50011 (hliu@iastate.edu).

**Institute for Analysis and Numerics, Otto-von-Guericke University Magdeburg, Universitätsplatz 2, 39106 Magdeburg, Germany (warnecke@ovgu.de).

Here the variables $x \geq 0$ and $t \geq 0$ denote the size of the particles and time, respectively. The number density of particles of size x at time t is denoted by $f(t, x)$. The coagulation kernel $K(x, y) \geq 0$ represents the rate at which the particles of size x coalesce with particles of size y and is assumed to be symmetric, i.e. $K(x, y) = K(y, x)$. Later, analogous models for breakage or fragmentation were developed. The continuous version of the coagulation and multiple fragmentation equations has been investigated, one of the models is of the form

$$(1) \quad \partial_t f(t, x) = \frac{1}{2} \int_0^x K(x-y, y) f(t, x-y) f(t, y) dy - \int_0^\infty K(x, y) f(t, x) f(t, y) dy \\ + \int_x^\infty b(x, y) S(y) f(t, y) dy - S(x) f(t, x).$$

Here the breakage function $b(x, y)$ is the probability density function for the formation of particles of size x from the particles of size y . It is non-zero only for $x < y$. The selection function $S(x)$ describes the rate at which particles of size x are selected to break. The selection function S and breakage function b are defined in terms of the multiple-fragmentation kernel $\Gamma(x, y)$ as

$$S(x) = \int_0^x \frac{y}{x} \Gamma(x, y) dy, \quad b(x, y) = \Gamma(y, x) / S(y).$$

This equation is usually referred as the generalized coagulation-fragmentation equation, as fragmenting particles can split into more than two pieces. Under some growth conditions solutions are shown to exist in the space

$$X = \left\{ f \in L^1 : \int_0^\infty (1+x) f dx < \infty, f \geq 0 \text{ a.e.} \right\}$$

for non-negative initial data $f_0 \in X$.

In aggregation-breakage processes the total number of particles varies in time while the total mass of particles remains conserved. In terms of f , the total number of particles and the total mass of particles at time $t \geq 0$ are respectively given by the moments

$$M_0(t) := \int_0^\infty f(t, x) dx, \quad M_1(t) := \int_0^\infty x f(t, x) dx.$$

It is easy to show that the total number of particles $M_0(t)$ decreases by aggregation and increases by breakage processes while the total mass $M_1(t)$ does not vary during these events. The total mass conservation

$$M_1(t) = M_1(0)$$

holds. However, for some special cases of K when it is sufficiently large compared to the selection function S , a phenomenon called gelation which has to do with a phase transition occurs. In this case the total mass of particles is not conserved, see Escobedo et al. [5] and further citations for details.

Mathematical results on existence and uniqueness of solutions of the equation (1) and further citations can be found in McLaughlin et al. [20] and Lamb [14] for rather general aggregation kernels, breakage and selection functions. However, the equation can only be solved analytically for a limited number of simplified problems, see Ziff [30], Dubovskii et al. [2] and the references therein. This leads to the necessity of using numerical methods for solving general equations. Several such numerical methods have been introduced. Stochastic methods (Monte-Carlo) have been developed, see Lee and Matsoukas [15] for solving equations of aggregation with binary breakage. Finite element techniques can be found in Mahoney and Ramkrishna [18] and the references therein for the equations of simultaneous aggregation, growth and nucleation. Some other numerical techniques are available in the literature such as the method of successive approximations by Ramkrishna [24], method of moments [17, 19], finite volume methods [21, 10],

and sectional methods, as the Fixed Pivot and the Cell Average Technique [9, 12, 28], to solve such PBEs. There also exist spline methods [3] and a DG method [25] for the aggregation process. All these methods are applied to the standard form of the aggregation-breakage equation and have to deal with the problem of mass conservation.

An alternative numerical approach is based on the mass balance formulation. An application of a Finite Volume Scheme (FVS) was introduced by Filbet and Laurençot [6] for solving the aggregation problem. Further, Bourgade and Filbet [1] have extended their scheme to solve the case of binary aggregation and binary breakage PBEs. For a special case of a uniform mesh they have shown error estimates of first order. The scheme has also been extended to two-dimensional aggregation problems by Qamar and Warnecke [23]. Finally it has been observed that the FVS is a good alternative to the methods mentioned above for solving the PBEs due to its automatic mass conservation property. An analysis of the finite volume method to solve the aggregation with multiple breakage PBEs on general meshes is given in [11]. The DG method presented in this work may be seen as a natural extension of the above FVSs.

This paper is organized as follows. First, we derive the DG scheme to solve aggregation-breakage PBEs in Section 2. Then in Section 3 details of the implementation are given. Later on, the scheme is numerically tested for several problems in Section 4. Further, Section 5 summarizes some conclusions.

2. METHOD DESCRIPTION

In this section a discontinuous Galerkin (DG) method for solving aggregation-breakage PBEs is discussed. Following [6] for aggregation, a new form of the breakage PBE is presented in order to apply the DG method efficiently.

2.1. Conservation formulation. Writing the aggregation and breakage terms in divergence form enables us to get a precise amount of mass dissipation or conservation. It can be written in a conservative form of mass density $n(t, x) = xf(t, x)$,

$$(2) \quad \partial_t n(t, x) + \partial_x (F_a(t, x) + F_b(t, x)) = 0, \quad n(0, x) = n_0(x) \geq 0 \text{ a.e.},$$

where the aggregation flux is

$$F_a(t, x) = \int_0^x \int_{x-u}^\infty A(u, v) n(t, u) n(t, v) dv du, \quad A(u, v) = K(u, v)/v,$$

and the breakage flux is

$$F_b(t, x) = - \int_x^\infty \int_0^x B(u, v) n(t, v) du dv, \quad B(u, v) = ub(u, v)S(v)/v.$$

It should be noted that both forms of aggregation-breakage PBEs (1) and (2) are interchangeable by using the Leibniz integration rule. It should also be mentioned that the equation (2) reduces to the case of pure aggregation or pure breakage process when F_b or F_a is zero, respectively.

In the PBE (2) the volume variable x ranges from 0 to ∞ . In order to apply a numerical scheme for the solution of the equation a first step is to truncate the problem and fix a finite computational domain $\Omega := [0, L]$ for an $0 < L < \infty$.

2.2. DG formulation. Discontinuous Galerkin (DG) methods are a class of finite element schemes used to solve mainly conservative PDEs.

We develop a discontinuous Galerkin (DG) method for (2) subject to initial data $n_0(x)$. Let us partition the interval $\Omega = [0, L]$ into $0 = x_{1/2}, x_{3/2}, \dots, x_{N+1/2} = L$ to get N subintervals and denote each cell by $I_j = (x_{j-1/2}, x_{j+1/2}]$, $j = 1, \dots, N$. Each cell has the length $h_j = x_{j+1/2} - x_{j-1/2}$ and we set $h = \max_j h_j$ to be the mesh size. The representative of each cell, usually the center of each cell, $x_j = \frac{1}{2}(x_{j-1/2} + x_{j+1/2})$, is called pivot or grid point. The

piecewise polynomial space V_h^k is defined as the space of polynomials of degree up to k in each cell I_j , that is,

$$(3) \quad V_h^k = \{v : v|_{I_j} \in P^k(I_j), j = 1, \dots, N\}.$$

Note that functions in V_h^k are allowed to have discontinuities across cell interfaces.

The DG scheme is defined as follows: find $n_h \in V_h^k$ such that

$$(4) \quad \int_{I_j} \partial_t n_h \phi dx - \int_{I_j} F \partial_x \phi dx + F \phi|_{\partial I_j} = 0, \quad F = F_a + F_b$$

for all test functions ϕ in the finite element space V_h^k . Here we use the notation, $v|_{\partial I_j} = v(x_{j+1/2}^-) - v(x_{j-1/2}^+)$, and $F_{j+1/2}$ is an appropriate approximation of the continuous flux function $F(t, x_{j+1/2})$. In case of a breakage process, the numerical flux may be approximated from the mass flux F_b ; Similarly for the aggregation problem with flux F_a . In general, we have $F_{j+1/2} = F_{a,j+1/2} + F_{b,j+1/2}$. The initial condition $n_h(0, x) \in V_h^k$ is generated by the piecewise L^2 projection of $n_0(x)$, that is

$$\int_0^L (n_h(0, x) - n_0(x)) \phi(x) dx = 0 \quad \text{for any } \phi \in V_h^k.$$

The semi-discrete DG scheme (4) is complete.

2.3. Flux evaluation. For the numerical integration of the fluxes we use Gaussian quadrature of order Q with the Gauss evaluation points $s_\alpha \in (-1, 1)$ and the weights $\omega_\alpha > 0$

$$(5) \quad \int_a^b g(u) du = \frac{b-a}{2} \int_{-1}^1 g\left(\frac{b+a}{2} + \frac{b-a}{2}s\right) ds = \frac{b-a}{2} \sum_{\alpha=1}^Q \omega_\alpha g\left(\frac{b+a}{2} + \frac{b-a}{2}s_\alpha\right) + R_Q,$$

where $R_Q = \mathcal{O}((b-a)^{2Q})$ is the approximation residual, which is zero when g is a polynomial of degree at most $2Q-1$. We will later use $Q = k+1$, see Remark 2.1.

First, consider the boundary term in the DG scheme (4). Denote the quadrature points in I_j as $\hat{x}_j^\alpha = x_j + \frac{h_j}{2}s_\alpha$ for $\alpha = 1, \dots, Q$. Then the aggregation flux

$$F_a(t, x_{j+1/2}) = \int_0^{x_{j+1/2}} \int_{x_{j+1/2}-u}^{x_{N+1/2}} A(u, v) n_h(t, u) n_h(t, v) dv du = \sum_{l=1}^j \int_{I_l} n_h(t, u) \Gamma_j(u) du$$

with the partial flux

$$\Gamma_j(u) = \int_{x_{j+1/2}-u}^{x_{N+1/2}} A(u, v) n_h(t, v) dv$$

is approximated by the numerical flux

$$(6) \quad F_{a,j+1/2} = \sum_{l=1}^j \frac{h_l}{2} \sum_{\alpha=1}^Q \omega_\alpha n_h(t, \hat{x}_l^\alpha) \Gamma_{j,l}^\alpha,$$

where $\Gamma_{j,l}^\alpha$ is an approximation to the partial flux $\Gamma_j(\hat{x}_l^\alpha)$ applying Gaussian quadrature rules, which we explain below. Let the index J be chosen such that $x_{j+1/2} - \hat{x}_l^\alpha \in I_J$, that is, $x_{J-1/2} < x_{j+1/2} - \hat{x}_l^\alpha \leq x_{J+1/2}$, then

$$\Gamma_j(\hat{x}_l^\alpha) = \int_{x_{j+1/2}-\hat{x}_l^\alpha}^{x_{J+1/2}} A(\hat{x}_l^\alpha, v) n_h(t, v) dv + \sum_{i=J+1}^N \int_{I_i} A(\hat{x}_l^\alpha, v) n_h(t, v) dv.$$

By the Gaussian quadrature formula (5), the integral terms can be approximated as

$$(7) \quad \Gamma_{j,l}^\alpha = \frac{1}{2}(b_J - a_J) \sum_{\beta=1}^Q \omega_\beta A(\hat{x}_l^\alpha, y_J^\beta) n_h(t, y_J^\beta) + \sum_{i=J+1}^N \frac{h_i}{2} \sum_{\beta=1}^Q \omega_\beta A(\hat{x}_l^\alpha, \hat{x}_i^\beta) n_h(t, \hat{x}_i^\beta),$$

where $a_J = x_{j+1/2} - \hat{x}_l^\alpha$, $b_J = x_{J+1/2}$ and the quadrature points in the first term are given by

$$y_J^\beta = \frac{1}{2}(b_J + a_J) + \frac{1}{2}(b_J - a_J)s_\beta.$$

To be more precise, the index J depends on j , l and α . Note, that in (7) the polynomial function n_h has to be evaluated at intermediate points y_J^β for the approximation of the integral part here.

Next, we evaluate the breakage flux

$$F_b(t, x_{j+1/2}) = - \int_{x_{j+1/2}}^{x_{N+1/2}} \int_0^{x_{j+1/2}} B(u, v) n_h(t, v) du dv = - \sum_{l=j+1}^N \int_{I_l} n_h(t, v) G_j(v) dv$$

with the partial flux

$$G_j(v) = \sum_{i=1}^j \int_{I_i} B(u, v) du$$

by the numerical flux

$$(8) \quad F_{b,j+1/2} = - \sum_{l=j+1}^N \frac{h_l}{2} \sum_{\alpha=1}^Q \omega_\alpha n_h(t, \hat{x}_l^\alpha) G_{j,l}^\alpha$$

where $G_{j,l}^\alpha$ is an approximation to the partial flux $G_j(\hat{x}_l^\alpha)$ and is given by

$$(9) \quad G_{j,l}^\alpha = \sum_{i=1}^j \frac{h_i}{2} \sum_{\beta=1}^Q \omega_\beta B(\hat{x}_i^\beta, \hat{x}_l^\alpha).$$

Now, let us consider the second term in the DG scheme (4). We apply again Gaussian quadrature of order Q for the approximation of the integral,

$$(10) \quad \int_{I_j} F \partial_x \phi dx = \int_{-1}^1 F \partial_\xi \phi d\xi = \sum_{\gamma=1}^Q \omega_\gamma \phi'(s_\gamma) F(t, \hat{x}_j^\gamma).$$

The approximation of the flux at the Gauss points, $F(t, \hat{x}_j^\gamma)$, is very similar to the approximation of the boundary terms above and is shown in the Appendix.

Remark 2.1. For the approximation of the integral over a cell I_j , we consider the Q -point Gaussian quadrature which is accurate for polynomials up to degree $2Q - 1$. In case of a linear and local flux function, F would be of polynomial degree k and ϕ' has maximal degree $k - 1$, in total $2k - 1$, corresponding to $Q = k$ Gauss points. In our case, the flux is non-local, quadrature rules are also needed for the evaluation of the flux. Note that $Q = k$ would be enough to make the scheme consistent. However, for our simulations we have chosen $Q = k + 1$ since we observe an interesting type of superconvergence in this case which we will demonstrate in the numerical tests, see Section 4. For simplicity, we choose the same Q for the numerical approximation of the partial fluxes which is not necessary.

2.4. Time discretization and positivity. By taking the Forward Euler discretization in time to (4), we obtain a fully discrete scheme

$$(11) \quad \int_{I_j} \frac{n_h^{m+1} - n_h^m}{\Delta t} \phi dx - \int_{I_j} F^m \phi_x dx + F^m \phi|_{\partial I_j} = 0.$$

Define the cell average of $n_h(x)$ on I_j by

$$(12) \quad \bar{n}_j := \frac{1}{h_j} \int_{I_j} n_h(x) dx.$$

Let $\phi = \frac{\Delta t}{h_j}$ so that

$$(13) \quad \bar{n}_j^{m+1} = \bar{n}_j^m - \lambda_j [F_{j+1/2}^m - F_{j-1/2}^m], \quad \lambda_j = \Delta t / h_j.$$

Due to the exactness of quadrature rule for polynomials of degree $2k+1$, and especially of degree k , we have

$$(14) \quad \bar{n}_j^m = \frac{1}{h_j} \int_{I_j} n_h^m(x) dx = \frac{1}{2} \sum_{\alpha=1}^Q \omega_\alpha n_h^m(\hat{x}_j^\alpha).$$

For the proof of the following theorem we take a closer look at the differences of the flux at two neighboring interfaces. The flux difference for F_a at time level m can be reorganized to

$$F_{a,j+1/2}^m - F_{a,j-1/2}^m = - \sum_{l=1}^{j-1} \frac{h_l}{2} \sum_{\alpha=1}^Q \omega_\alpha n_h^m(\hat{x}_l^\alpha) (\Gamma_{j-1,l}^\alpha - \Gamma_{j,l}^\alpha) + \frac{h_j}{2} \sum_{\alpha=1}^Q \omega_\alpha n_h^m(\hat{x}_j^\alpha) \Gamma_{j,j}^\alpha,$$

where the two terms on the right hand side can be seen as a type of birth and death term, respectively. For the use in the following theorem, define the first term as

$$B_{a,j} = \sum_{l=1}^{j-1} \frac{h_l}{2} \sum_{\alpha=1}^Q \omega_\alpha n_h^m(\hat{x}_l^\alpha) (\Gamma_{j-1,l}^\alpha - \Gamma_{j,l}^\alpha).$$

Similarly, the flux difference for F_b at time level m can be combined to

$$F_{b,j+1/2}^m - F_{b,j-1/2}^m = - \sum_{l=j+1}^N \frac{h_l}{2} \sum_{\alpha=1}^Q \omega_\alpha n_h^m(\hat{x}_l^\alpha) (G_{j,l}^\alpha - G_{j-1,l}^\alpha) + \frac{h_j}{2} \sum_{\alpha=1}^Q \omega_\alpha n_h^m(\hat{x}_j^\alpha) G_{j-1,j}^\alpha.$$

Note, that $G_{j,l}^\alpha - G_{j-1,l}^\alpha \geq 0$ and $G_{j-1,j}^\alpha \geq 0$.

Theorem 2.1. *The high order scheme (13) preserves the positivity, i.e., assuming the numerical solution at time level t_m positive, then $\bar{n}_j^{m+1} > 0$ under the CFL condition*

$$(15) \quad \Delta t < \frac{1}{\max_{j,\alpha} \left((\Gamma_{j,j}^\alpha)_+ + G_{j-1,j}^\alpha + \frac{1}{h_j \bar{n}_j^m} (-B_{a,j})_+ \right)},$$

where $(\cdot)_+$ denotes $\max\{\cdot, 0\}$. In particular, if n_h^m is positive at all points \hat{x}_j^α , then $\bar{n}_j^{m+1} > 0$.

Proof. We rewrite scheme (13), using (14), as

$$\begin{aligned}
\bar{n}_j^{m+1} &= \frac{1}{2} \sum_{\alpha=1}^Q \omega_{\alpha} n_h^m(\hat{x}_j^{\alpha}) - \lambda_j [F_{j+1/2} - F_{j-1/2}] \\
&= \frac{1}{2} \sum_{\alpha=1}^Q \omega_{\alpha} n_h^m(\hat{x}_j^{\alpha}) - \lambda_j \left[\frac{h_j}{2} \sum_{\alpha=1}^Q \omega_{\alpha} n_h^m(\hat{x}_j^{\alpha}) \Gamma_{j,j}^{\alpha} - \sum_{l=1}^{j-1} \frac{h_l}{2} \sum_{\alpha=1}^Q \omega_{\alpha} n_h^m(\hat{x}_l^{\alpha}) (\Gamma_{j-1,l}^{\alpha} - \Gamma_{j,l}^{\alpha}) \right] \\
&\quad - \lambda_j \left[\frac{h_j}{2} \sum_{\alpha=1}^Q \omega_{\alpha} n_h^m(\hat{x}_j^{\alpha}) G_{j-1,j}^{\alpha} - \sum_{l=j+1}^N \frac{h_l}{2} \sum_{\alpha=1}^Q \omega_{\alpha} n_h^m(\hat{x}_l^{\alpha}) (G_{j,l}^{\alpha} - G_{j-1,l}^{\alpha}) \right] \\
&\geq \frac{1}{2} \sum_{\alpha=1}^Q \omega_{\alpha} n_h^m(\hat{x}_j^{\alpha}) \left[1 - \Delta t \Gamma_{j,j}^{\alpha} - \Delta t G_{j-1,j}^{\alpha} - \Delta t \frac{1}{h_j \bar{n}_j^m} (-B_{a,j}) \right].
\end{aligned}$$

Therefore, $\bar{n}_j^{m+1} > 0$ under the restriction on the time step (15). \square

Remark 2.2. The CFL condition is somewhat inconvenient, but this condition is only sufficient. For aggregation, in most practical cases the term $B_{a,j}$ is positive, hence the third term of the condition vanishes. For breakage, the condition depends only on the breakage kernel and the maximal grid point, what forces the time step to be very small. Fortunately, in most cases the time step can be chosen much larger without losing positivity.

Remark 2.3. Ideally the assumption should be $n_h \geq 0$. In fact, the theorem can be relaxed to $n_h^m \geq 0$ at all quadrature points \hat{x}_j^{α} requiring only strictly positive cell averages, $\bar{n}_j^m > 0$.

2.5. A scaling limiter. Theorem 2.1 implies that in order to preserve the solution positivity, we need to enforce $n_h^m(\hat{x}_j^{\alpha}) \geq 0$. This is achieved by a reconstruction step using cell averages as a reference.

Let $n_h \in P^k(I_j)$ be an approximation of a smooth function $n(x) \geq 0$ with the cell average \bar{n}_j , defined in (12). Following the idea of scaling limiter by [29], we define the scaled polynomial by

$$(16) \quad \tilde{n}_h(x) = \theta (n_h(x) - \bar{n}_j) + \bar{n}_j, \quad \theta = \min \left\{ 1, \frac{\bar{n}_j}{\bar{n}_j - \min_{x \in I_j} n_h(x)} \right\}.$$

It is easy to check that the cell average of \tilde{n}_h is still \bar{n}_j and $\tilde{n}_h \geq 0$ in I_j . Following [29, 16], we have the next lemma.

Lemma 2.2. *If $\bar{n}_j > 0$, then the modified polynomial is as accurate as n_h in the following sense*

$$(17) \quad |\tilde{n}_h(x) - n_h(x)| \leq C_k \|n_h - n\|_{\infty} \quad \text{for all } x \in I_j,$$

where C_k is a constant depending on the polynomial degree k .

Remark 2.4. Since we only need control of the values at the Gaussian quadrature points

$$S_j = \{\hat{x}_j^{\alpha}, \alpha = 1, \dots, Q\}$$

we could replace (16) by

$$(18) \quad \theta = \min \left\{ 1, \frac{\bar{n}_j}{\bar{n}_j - \min_{x \in S_j} n_h(x)} \right\}$$

and the limiter (16) with (18) is sufficient to ensure

$$\tilde{n}_h(x) \geq 0 \quad \text{for all } x \in S_j.$$

Furthermore, Lemma 2.2 remains valid with this less restrictive limiter, i.e., we have

$$|\tilde{n}_h(x) - n_h(x)| \leq C_k \|n_h - n\|_\infty \quad \text{for all } x \in I_j,$$

where C_k is a constant depending on k .

Remark 2.5. Lemma 2.2 establishes that the reconstructed polynomial is as accurate as the original polynomial. Our numerical results based on this reconstruction are excellent. It would be interesting to analyze how the reconstruction error will accumulate in time.

3. IMPLEMENTATION DETAILS

3.1. Matrix formulation and implementation. We would like to introduce the matrix formulation of our numerical scheme and outline the flowchart of the algorithm.

As a basis for the set of test functions we choose the Legendre polynomials, denoted by $\phi_i(\xi)$,

$$\phi_0(\xi) = 1, \quad \phi_1(\xi) = \xi, \quad \phi_2(\xi) = \frac{1}{2}(3\xi^2 - 1), \dots \quad \phi := (\phi_0, \dots, \phi_k)^T,$$

which are orthogonal in $L^2([-1, 1])$. On each cell, the unknown function can be represented as

$$n_h(t, x) = \sum_{i=0}^k n_j^i(t) \phi_i(\xi^j(x)), \quad x \in I_j.$$

Here $\xi^j(x)$ is the mapping from I_j to $[-1, 1]$, $\xi^j(x) := \frac{2}{h_j}(x - x_j)$. To determine n_h , it suffices to identify the coefficients $n_j = (n_j^0, \dots, n_j^k)^T$. Due to the orthogonality of the basis functions the mass matrix becomes diagonal,

$$(19) \quad \int_{I_j} \partial_t n_h \phi \, dx = \frac{h_j}{2} \int_{-1}^1 \phi(\xi) \phi^T(\xi) d\xi \frac{d}{dt} n_j(t) = \frac{h_j}{2} \text{diag}\{c_0, \dots, c_k\} \frac{d}{dt} n_j(t),$$

where $c_i = \frac{2}{2i+1}$ are the normalization constants.

The fact that we only require n_h^m be nonnegative at certain points can reduce the computational cost considerably. Instead of finding the minimum of n_h on the whole computational cell I_j , we take the minimum only on the test set S_j .

3.2. Algorithm flowchart. For simplicity, we only consider the Euler forward time stepping. The algorithm with the strong stability preserving (SSP) Runge-Kutta method [7] for higher order time discretization can be implemented by repeating the following flowchart in each stage; since each SSP-RK method is a convex linear combination of the forward Euler. The desired positivity preserving property is ensured under a suitable CFL condition.

- (1) Initialization: From the given initial data $n_0(x)$
 - (i) generate $n_h^0 \in V_h^k$ by piecewise L^2 projection,
 - (ii) reconstruct n_h^0 as in step 3.
- (2) Evolution: Use the scheme (11) to compute n_h^{m+1} .
 - (i) If \bar{n}_j^{m+1} is positive for all j , set $n_h^m = n_h^{m+1}$, continue with step 3.
 - (ii) Otherwise, halve the time step Δt and restart step 2.
- (3) Reconstruction: Use (16) with (18) and set $n_h^m = \tilde{n}_h^m$, continue with step 2.

4. NUMERICAL RESULTS

In this section, we give numerical tests for the proposed positivity-preserving DG scheme applied to pure aggregation, breakage and also for the combined processes considering several test problems. The following test cases are chosen similar to those in [11]. We compare our results with some standard numerical methods, the Cell Average Technique (CAT) by J. Kumar [9] and the Finite Volume Scheme (FVS) by Filbet and Laurengot [6] which is a special case of

the presented DG scheme for $k = 0$. The error calculation for the Cell Average Technique is based on the number density, $f(t, x)$, whereas all other errors are calculated with respect to the mass density, $n(t, x) = xf(t, x)$.

For this type of equations it is convenient to use a geometric grid, $x_{j+1/2} = rx_{j-1/2}$. We choose the factor $r = 2^{(30/N)}$ to span about 9 orders of magnitude. We set $x_{1/2} = 0$ and $x_{3/2} = x_0$ where x_0 can be adapted to the different cases.

All numerical simulations below were carried out to investigate the experimental order of convergence (EOC). The error is measured in a continuous and a discrete norm. The continuous L^1 norm can be approximated by

$$(20) \quad e_h = \sum_j \frac{h_j}{2} \sum_{\alpha=1}^R \tilde{\omega}_\alpha |n_h(t, \tilde{x}_j^\alpha) - n(t, \tilde{x}_j^\alpha)|,$$

using a high-order Gaussian quadrature rule, where $\tilde{\omega}_\alpha > 0$ are the weights, and \tilde{x}_j^α are the corresponding Gauss points in each cell I_j . We choose $R = 16$ through all the examples. The symbol h corresponds to the number of cells. The discrete L^1 norm is given by

$$(21) \quad e_{h,d} = \sum_j \frac{h_j}{2} \sum_{\alpha=1}^Q \omega_\alpha |n_h(t, \hat{x}_j^\alpha) - n(t, \hat{x}_j^\alpha)|,$$

where the Gaussian quadrature points are the same as used for the discretization of the scheme. We have chosen the L^1 norm since it is a natural choice for conservation laws. Using the L^2 or L^∞ norm, similar numerical results and the same order of convergence can be obtained. The error calculation in the discrete norm coincides for $k = 0$ with that used by Filbet and Laurençot [6] for the Finite Volume Scheme.

If the problem has analytical solutions, the following formula is used to calculate the EOC

$$\text{EOC} = \ln(e_h/e_{h/2})/\ln(2).$$

In case of unavailability of the analytical solutions, the EOC can be computed using $e_h = \|n_h - n_{h/2}\|$ where $n_{h/2}$ is interpolated onto the grid of n_h by a high order interpolation method. For the calculation of the EOC we show the numerical errors at time $t = 0.01$ since the order of convergence of the DG scheme after longer times is disturbed by the low order time integration.

We shall also evaluate the moments of the numerical solution by

$$M_{p,h} = \int_0^L x^{p-1} n_h(t, x) dx = \sum_j \frac{h_j}{2} \sum_{\alpha=1}^R \tilde{\omega}_\alpha (\tilde{x}_j^\alpha)^{p-1} n_h(t, \tilde{x}_j^\alpha), \quad p = 0, 1, 2, \dots,$$

where R is chosen large enough such that the integration is exact for all moments under consideration. The error in the moments is then given by

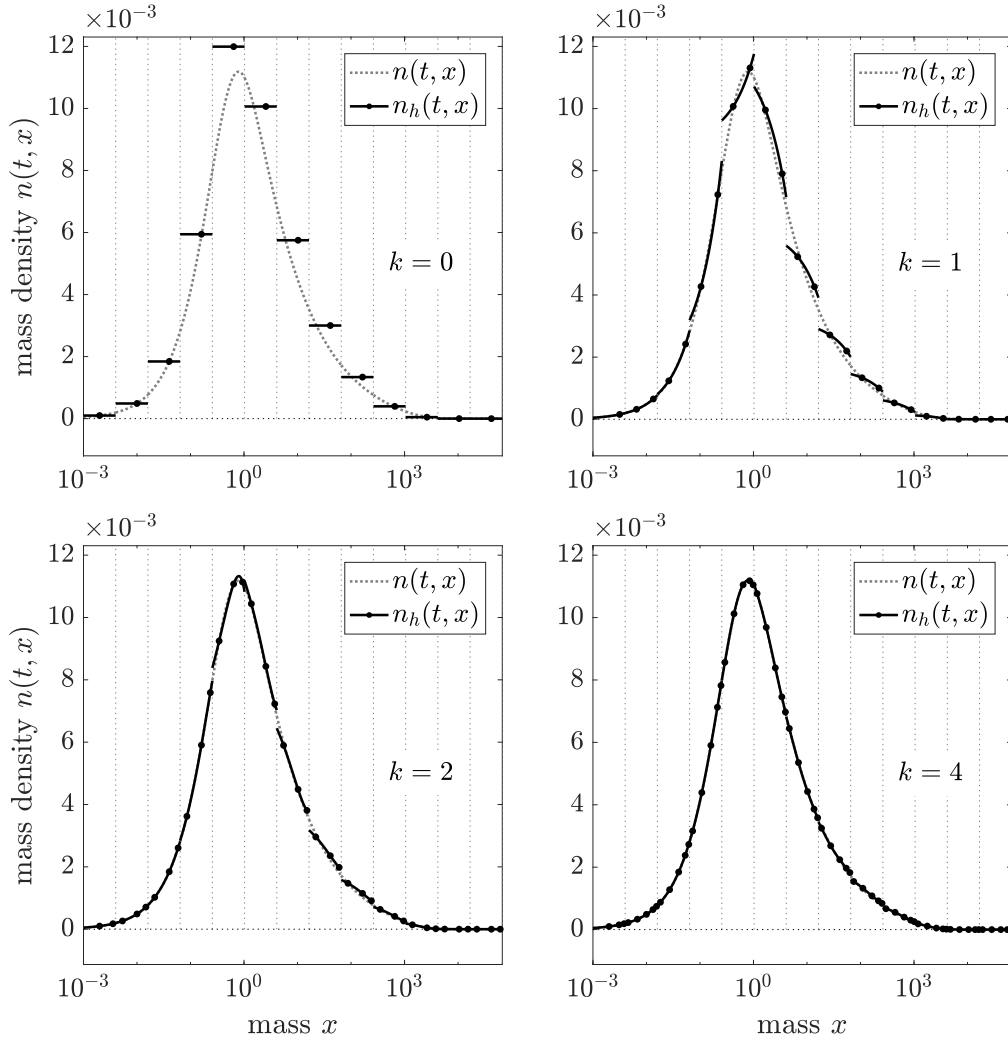
$$e(M_{p,h}) = \frac{|M_{p,h} - M_p|}{M_p}, \quad p = 0, 1, 2, \dots$$

where the error in the first moment $e(M_{1,h})$ of course vanishes by construction of the method.

4.1. Pure aggregation. Test case 1:

The numerical verification of the EOC of the DG solutions for aggregation is discussed by taking three problems, namely the case of constant, sum and product aggregation kernels. The analytical solutions for these problems taking the exponential initial distribution $n(0, x) = x \exp(-x)$ have been given in Scott [26]. The computational domain in these cases is taken as $[10^{-3}, 10^6]$.

The numerical solutions for the sum aggregation kernel with $N = 15$ cells and different polynomial degree k are shown in Figure 1. The numerical solution is shown together with the analytical one at time $t = 3$ where the degree of aggregation is $I_{\text{agg}} = 1 - M_0(t)/M_0(0) \approx 95\%$.

FIGURE 1. Numerical solution for $N = 15$ cells and different k for test case 1

Due to the logarithmic scale of the x -axis the piecewise linear solution for $k = 1$ appears curved and also the Gauss points are of course symmetrically distributed in one cell. Obviously, the approximation improves for a higher polynomial degree.

$k \backslash N$	15	30	60	120	240	EOC
0 (FVS)	4.2e-1	2.1e-1	1.0e-1	5.2e-2	2.6e-2	1.0
1	1.3e-1	4.4e-2	1.1e-2	2.8e-3	6.9e-4	2.0
2	7.4e-2	8.0e-3	1.1e-3	1.4e-4	1.7e-5	3.0
4	1.3e-2	3.0e-4	1.0e-5	3.3e-7	1.0e-8	5.0
8	3.6e-5	3.7e-7	7.0e-10	1.4e-12	1.2e-14	9.0
CAT	5.3e-1	2.3e-1	1.1e-1	5.3e-2	2.6e-2	1.0

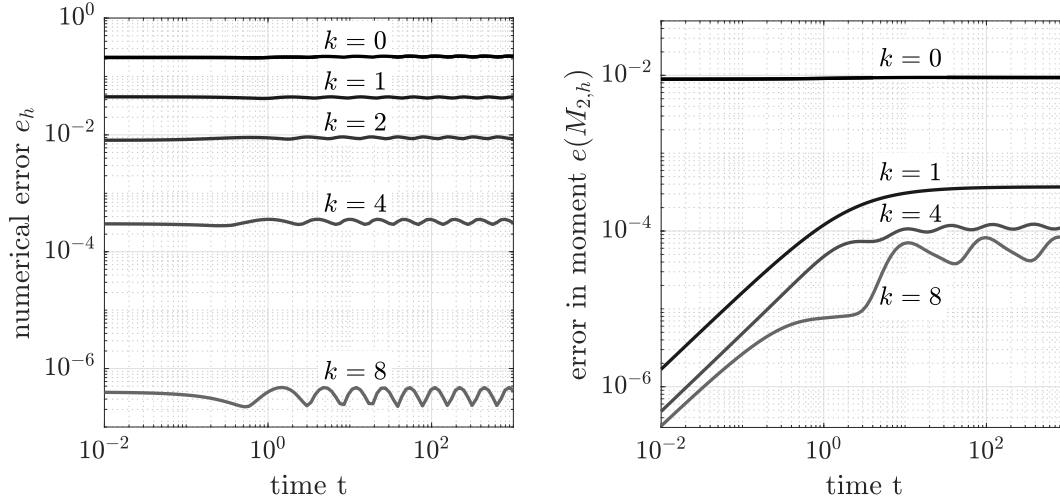
TABLE 1. L^1 errors e_h and EOC for test case 1

$k \backslash N$	15	30	60	120	240	EOC
0 (FVS)	1.3e-1	5.5e-2	1.4e-2	3.5e-3	8.8e-4	2.0
1	8.7e-2	9.0e-3	1.2e-3	1.5e-4	1.8e-5	3.0
2	3.8e-2	1.9e-3	1.1e-4	6.8e-6	4.3e-7	4.0
4	3.6e-3	5.2e-5	9.4e-7	1.5e-8	2.3e-10	6.0
8	2.9e-5	4.7e-8	6.0e-11	6.6e-14	2.0e-14	10.0
CAT	1.3e-1	3.7e-2	9.6e-3	2.4e-3	6.1e-4	2.0

TABLE 2. Discrete L^1 errors $e_{h,d}$ and EOC for test case 1

The numerical errors for the sum aggregation kernel are shown in Table 1 and Table 2. In the continuous L^1 norm the EOC is $k + 1$ as expected. In the discrete L^1 norm the EOC is $k + 2$ on a geometric grid which is one order higher than in the continuous norm. It appears that the evaluation of the numerical solution at the same Gauss points as used for the discretization of the scheme shows a type of superconvergence. For $k = 0$, the second order convergence for the Finite Volume Scheme on smooth grids was proven in [11].

The numerical results for the constant and product aggregation kernels are very similar and are not shown again. In our tests we observe that even the post-gelation phase, see e.g. [4], for the product aggregation kernel can be simulated very well.

FIGURE 2. Error evolution of the numerical solution (left) and of the second moment (right) for different k for test case 1

The evolution of the numerical error in time is shown for the constant aggregation kernel in Figure 2 (left). We show the results for $N = 30$ cells and varying polynomial degree k up to time $t = 1000$ where the degree of aggregation is $I_{\text{agg}} \approx 99.8\%$. One can observe that the numerical error remains bounded for longer times.

In this test case, we also discuss the approximation of the moments. The error in the first 6 moments M_0, \dots, M_5 for the constant aggregation kernel at time $t = 1000$ are shown in Table 3. For a better comparison we have chosen the same number of evaluation points $N(k+1) = 90$. One can see that the prediction of the zeroth moment is very accurate and even the higher moments are approximated well. The lower moments are predicted better for an increasing polynomial

(N, k)	$e(M_{0,h})$	$e(M_{1,h})$	$e(M_{2,h})$	$e(M_{3,h})$	$e(M_{4,h})$	$e(M_{5,h})$
FVS (90, 0)	6.6e-3	0	9.4e-3	3.7e-2	8.6e-2	1.6e-1
(45, 1)	2.8e-4	0	3.7e-4	3.8e-3	1.6e-2	4.5e-2
(30, 2)	6.7e-5	0	6.2e-4	2.2e-3	3.6e-3	1.5e-3
(18, 4)	9.1e-6	0	1.2e-4	6.1e-4	3.1e-3	1.6e-2
(10, 8)	5.1e-6	0	7.7e-5	7.6e-4	8.2e-3	4.6e-2
CAT (90)	3.7e-14	0	1.1e-2	2.9e-2	5.1e-2	7.3e-2

TABLE 3. Numerical errors in the first 6 moments for test case 1

degree k . The accuracy in the higher moments for a larger polynomial degree k is disturbed by some small oscillations of the piecewise high order polynomial for large values of x . For the Cell Average Technique (CAT) we have to use the normalized moments $\tilde{M}_{p,h}(t) = M_{p,h}(t)/M_{p,h}(0)$ for the error calculation of the moments, $e(\tilde{M}_{p,h})$, since the discretization is focused on the number density and even the first moment has a discretization error in the initial distribution. The first two moments are preserved exactly by construction of the method and it produces similar errors as the Finite Volume Scheme for the higher moments.

In Figure 2 (right) we have shown the evolution of the error in the second moment $e(M_{2,h})$ for different k again with the same number of evaluation points $N(k+1) = 90$ in time. One can observe that the error in the moments increases initially but remains bounded for longer times.

4.2. Pure breakage. Test case 2:

Here, the EOC is calculated for the binary breakage $b(x, y) = 2/y$ together with the linear and quadratic selection functions, i.e. $S(x) = x$ and $S(x) = x^2$. The analytical solutions for such problems have been given by Ziff and McGrady [31] for an exponential initial condition, $n(0, x) = x \exp(-x)$. The computational domain in these cases is taken as $[10^{-6}, 10^3]$.

$k \setminus N$	15	30	60	120	240	EOC
0 (FVS)	4.2e-1	2.1e-1	1.0e-1	5.2e-2	2.6e-2	1.0
1	1.3e-1	4.5e-2	1.1e-2	2.8e-3	6.9e-4	2.0
2	7.0e-2	8.0e-3	1.1e-3	1.4e-4	1.7e-5	3.0
4	1.3e-2	3.1e-4	1.0e-5	3.3e-7	1.0e-8	5.0
8	2.5e-5	4.2e-7	7.4e-10	1.4e-12	1.2e-14	9.0
CAT	5.3e-1	2.3e-1	1.1e-1	5.3e-2	2.6e-2	1.0

TABLE 4. L^1 errors e_h and EOC for test case 2

The results for the linear selection function are shown in Table 4. Hence, we observe that the DG scheme is $k+1$ order convergent in the L^1 norm. Similar to the previous case, the order of convergence is $k+2$ using the discrete L^1 norm which is not shown again. For $k=0$, the second order convergence was proven in [11] to be mesh-independent for breakage.

The results for the quadratic selection function are very similar and are omitted. Also the behavior of the error evolution and the error in the moments is similar and is not shown again.

Test case 3: Now the case of multiple breakage with the quadratic selection function $S(x) = x^2$ is considered where an analytical solution is not known. For the numerical simulations, the

following normal distribution as an initial condition is taken

$$n(0, x) = \frac{1}{\sigma\sqrt{2\pi}} \exp\left(-\frac{(x - \mu)^2}{2\sigma^2}\right).$$

The computations are made for the breakage function considered by Hill and Ng [8]

$$b(x, y) = p \left(\frac{[m + (m + 1)(p - 1)]!}{m![m + (m + 1)(p - 2)]!} \right) \frac{x^m(y - x)^{m+(m+1)(p-2)}}{y^{pm+p-1}}, \quad p \in \mathbb{N}, \quad p \geq 2,$$

where the relation $\int_0^y b(x, y) dx = p$ holds where p gives the total number of fragments per breakage event. The parameter $m \geq 0$ is responsible for the shape of the daughter particle distribution. The numerical solutions are obtained using $p = 4$, $m = 2$.

$k \setminus N$	15	30	60	120	240	EOC
0 (FVS)	5.5e-1	2.5e-1	1.1e-1	6.6e-2	3.3e-2	1.0
1	1.7e-1	5.5e-2	1.4e-2	3.5e-3	8.8e-4	2.0
2	3.0e-2	1.3e-2	1.6e-3	2.0e-4	2.6e-5	3.0
4	1.4e-2	5.8e-4	1.6e-5	5.6e-7	1.7e-8	5.0
8	4.0e-4	1.5e-7	1.6e-9	3.1e-12	8.2e-14	9.0
CAT	3.0e-1	1.1e-1	4.6e-2	2.1e-2	1.0e-2	1.0

TABLE 5. L^1 errors e_h and EOC for test case 3

For the numerical simulation the computational domain is taken as $[10^{-6}, 10^3]$. In this case, the numerical error e_h is computed from the numerical solutions n_h and $n_{h/2}$, as mentioned above. As expected, we again observe from Table 5 that the DG scheme shows convergence of order $k + 1$. Using the discrete L^1 norm we again obtain the higher convergence order $k + 2$.

4.3. Coupled aggregation-breakage. Test case 4:

Finally, the EOC is evaluated for the simultaneous process with a constant aggregation kernel $K(x, y) = 1$ and breakage kinetics $b(x, y) = 2/y$, $S(x) = x/2$. For the simulation the computational domain $[10^{-3}, 10^6]$ is taken. The analytical solutions for this problem are given by Lage [13] for the following two different initial conditions

$$\begin{aligned} n(0, x) &= xe^{-x}, \\ n(0, x) &= 4x^2e^{-2x}. \end{aligned}$$

The former exponential initial condition is a steady state solution. The latter Gaussian-like initial condition is a special case where the number of particles stays constant. From Table 6, we find that the DG scheme is $k + 1$ order convergent where the results for the first case are shown. As before, we obtain one order higher convergence on a geometric grid in the discrete norm. The second case is very similar and is omitted.

5. CONCLUDING REMARKS

In this paper, we have developed a high order DG scheme which can be proven to be positivity-preserving for both coagulation and fragmentation equations. We have tested the DG scheme and clearly observed the convergence order $k + 1$ and the strict positivity preservation in all these tests. Interestingly, the DG scheme shows a type of superconvergence of order $k + 2$ on a geometric grid in the discrete norm which evaluates the numerical solution at the same Gaussian quadrature points as used for the discretization of the scheme. Even though the CFL condition derived to preserve positivity might be very small in some cases, we emphasize that it is not a

$k \setminus N$	15	30	60	120	240	EOC
0 (FVS)	4.2e-1	2.1e-1	1.1e-1	5.2e-2	2.6e-2	1.0
1	1.3e-1	4.5e-2	1.1e-2	2.8e-3	6.9e-4	2.0
2	7.4e-2	8.1e-3	1.1e-3	1.4e-4	1.7e-5	3.0
4	1.3e-2	3.0e-4	1.0e-5	3.3e-7	1.0e-8	5.0
8	3.9e-5	4.0e-7	7.3e-10	1.4e-12	4.2e-15	9.0
CAT	5.3e-1	2.3e-1	1.1e-1	5.3e-2	2.6e-2	1.0

TABLE 6. L^1 errors e_h and EOC for test case 4

necessary condition and can be relaxed significantly. The high accuracy was verified numerically by taking various examples of pure aggregation, pure breakage and the combined problems.

By applying the limiter or the simplified version which avoids the evaluation of extrema of polynomials, to a discontinuous Galerkin scheme solving one dimensional coagulation-fragmentation equations, with the time evolution by a SSP Runge-Kutta method, we obtain a high order accurate scheme with strict positivity-preservation.

Acknowledgements. Liu's research was partially supported by the National Science Foundation under grant DMS-1312636, and DMS-1107291. Gröpler's research was partially supported by the German Research Foundation DFG, Research Training Group GRK 1554.

APPENDIX

In Section 2.3 we have shown the flux evaluation for the boundary term in the DG scheme (4). For the numerical approximation of the second term we apply Gaussian quadrature, as already shown in (10). The approximation of the flux at the Gauss points, $F(t, \hat{x}_j^\gamma)$, is shown in the following. For aggregation the flux $F_a(t, \hat{x}_j^\gamma)$ can be approximated by the numerical flux

$$(22) \quad F_{a,j}^\gamma = \sum_{l=1}^j \frac{b_l - a_l}{2} \sum_{\alpha=1}^Q \omega_\alpha n_h(t, u_l^\alpha) \Gamma_{j,l}^{\gamma,\alpha},$$

where $a_l = x_{l-1/2}$ and $b_l = x_{l+1/2}$ for $l < j$ and $b_l = \hat{x}_j^\gamma$ for $l = j$, and $u_l^\alpha = \frac{1}{2}(b_l + a_l) + \frac{1}{2}(b_l - a_l)s_\alpha$. The partial flux $\Gamma_{j,l}^\gamma(u_l^\alpha)$ is approximated by

$$(23) \quad \Gamma_{j,l}^{\gamma,\alpha} = \frac{1}{2}(b_J - a_J) \sum_{\beta=1}^Q \omega_\beta A(u_l^\alpha, y_J^\beta) n_h(t, y_J^\beta) + \sum_{i=J+1}^N \frac{h_i}{2} \sum_{\beta=1}^Q \omega_\beta A(u_l^\alpha, \hat{x}_i^\beta) n_h(t, \hat{x}_i^\beta),$$

where $a_J = \hat{x}_j^\alpha - u_l^\alpha$, $b_J = x_{J+1/2}$, and $y_J^\beta = \frac{1}{2}(b_J + a_J) + \frac{1}{2}(b_J - a_J)s_\beta$. The index J is chosen such that $\hat{x}_j^\gamma - u_l^\alpha \in I_J$. Here, the index J depends on j, γ, l and α .

For breakage the flux $F_b(t, \hat{x}_j^\gamma)$ is approximated by

$$(24) \quad F_{b,j}^\gamma = - \sum_{l=j}^N \frac{b_l - a_l}{2} \sum_{\alpha=1}^Q \omega_\alpha n_h(t, u_l^\alpha) G_{j,l}^{\gamma,\alpha},$$

where $a_l = \hat{x}_j^\gamma$ for $l = j$ and $a_l = x_{l-1/2}$ for $l > j$, $b_l = x_{l+1/2}$, and $u_l^\alpha = \frac{1}{2}(b_l + a_l) + \frac{1}{2}(b_l - a_l)s_\alpha$. The partial flux $G_{j,l}^\gamma(u_l^\alpha)$ is approximated by

$$(25) \quad G_{j,l}^{\gamma,\alpha} = \sum_{i=1}^j \frac{b_i - a_i}{2} \sum_{\beta=1}^Q \omega_\beta B(u_i^\beta, u_l^\alpha),$$

where $a_i = x_{i-1/2}$, $b_i = x_{i+1/2}$ for $i < j$ and $b_i = \hat{x}_j^\gamma$ for $i = j$, and $u_i^\beta = \frac{1}{2}(b_i + a_i) + \frac{1}{2}(b_i - a_i)s_\beta$.

REFERENCES

- [1] J.P. Bourgade and F. Filbet. Convergence of a finite volume scheme for coagulation-fragmentation equations. *Mathematics of Computation*, 77:851-882, 2007.
- [2] P.B. Dubovskii, V.A. Galkin and I.W. Stewart. Exact solutions for the coagulation-fragmentation equations. *Journal of Physics A: Mathematical and General*, 25(18):4737-4744, 1992.
- [3] L.D. Erasmus, D. Eyre and R.C. Everson. Numerical treatment of the population balance equation using a spline-Galerkin method. *Computers and Chemical Engineering*, 18(9):775-783, 1994.
- [4] M.H. Ernst, R.M. Ziff and E.M. Hendriks. Coagulation processes with a phase transition. *Journal of Colloid and Interface Science*, 97(1):266-277, 1984.
- [5] M. Escobedo, P. Laurençot, S. Mischler and B. Perthame. Gelation and mass conservation in coagulation-fragmentation models. *Journal of Differential Equations*, 195(1):143-174, 2003.
- [6] F. Filbet and P. Laurençot. Numerical simulation of the Smoluchowski coagulation equation. *SIAM Journal on Scientific Computing*, 25(6):2004-2028, 2004.
- [7] S. Gottlieb, C.-W. Shu and E. Tadmor. Strong stability-preserving high-order time discretization methods. *SIAM Review*, 43(1):89-112, 2001.
- [8] P.J. Hill and Ka M. Ng. Statistics of multiple particle breakage. *AIChE Journal*, 42(6):1600-1611, 1996.
- [9] J. Kumar. Numerical approximations of population balance equations in particulate systems. *Otto-von-Guericke University Magdeburg*, Germany, PhD thesis, 2006.
- [10] R. Kumar, J. Kumar and G. Warnecke. Moment preserving finite volume schemes for solving population balance equations incorporating aggregation, breakage, growth and source terms. *Mathematical Models and Methods in Applied Sciences*, 23(7):1235-1273, 2013.
- [11] R. Kumar, J. Kumar and G. Warnecke. Convergence analysis of a finite volume scheme for solving non-linear aggregation-breakage population balance equations. *Kinetic and Related Models*, 7(4):713-737, 2014.
- [12] S. Kumar and D. Ramkrishna. On the solution of population balance equations by discretization - I. A fixed pivot technique. *Chemical Engineering Science*, 51(8):1311-1332, 1996.
- [13] P.L.C. Lage. Comments on the "An analytical solution to the population balance equation with coalescence and breakage-the special case with constant number of particles" by D.P. Patil and J.R.G. Andrews. *Chemical Engineering Science*, 57(19):4253-4254, 2002.
- [14] W. Lamb. Existence and uniqueness results for the continuous coagulation and fragmentation equation. *Mathematical Methods in the Applied Sciences*, 27(6):703-721, 2004.
- [15] K. Lee and T. Matsoukas. Simultaneous coagulation and break-up using constant-N Monte Carlo. *Powder Technology*, 110(1-2):82-89, 2000.
- [16] H. Liu and H. Yu. Maximum-principle-satisfying third order discontinuous Galerkin schemes for Fokker-Planck equations. *SIAM Journal on Scientific Computing*, 36(5), A2296-A2325, 2014.
- [17] G. Madras and B.J. McCoy. Reversible crystal growth-dissolution and aggregation-breakage: numerical and moment solutions for population balance equations. *Powder Technology*, 143-144:297-307, 2004.
- [18] A.W. Mahoney and D. Ramkrishna. Efficient solution of population balance equations with discontinuities by finite elements. *Chemical Engineering Science*, 57(7):1107-1119, 2002.
- [19] D.L. Marchisio and R.O. Fox. Solution of population balance equations using the direct quadrature method of moments. *Journal of Aerosol Science*, 36(1):43-73, 2005.
- [20] D.J. McLaughlin, W. Lamb and A.C. McBride. Existence and uniqueness results for the non-autonomous coagulation and multiple-fragmentation equation. *Mathematical Methods in the Applied Sciences*, 21(11):1067-1084, 1998.
- [21] S. Motz, A. Mitrović and E.-D. Gilles. Comparison of numerical methods for the simulation of dispersed phase systems. *Chemical Engineering Science*, 57(20):4329-4344, 2002.
- [22] H. Müller. Zur allgemeinen Theorie der raschen Koagulation. *Kolloidchemische Beihefte*, 27:223-250, 1928.
- [23] S. Qamar and G. Warnecke. Solving population balance equations for two-component aggregation by a finite volume scheme. *Chemical Engineering Science*, 62(3):679-693, 2007.
- [24] D. Ramkrishna. Population balances. Theory and applications to particulate systems in engineering. *Academic Press*, San Diego, USA, 2000.
- [25] A. Sandu. Piecewise polynomial solutions of aerosol dynamic equation. *Aerosol Science and Technology*, 40(4):261-273, 2006.
- [26] W.T. Scott. Analytic studies of cloud droplet coalescence I. *Journal of the Atmospheric Sciences*, 25(1):54-65, 1968.

- [27] M. v. Smoluchowski. Versuch einer mathematischen Theorie der Koagulationskinetik kolloider Lösungen. *Zeitschrift für physikalische Chemie*, XCII:129-168, 1917.
- [28] M. Vanni. Approximate population balance equations for aggregation-breakage processes. *Journal of Colloid and Interface Science*, 221(2):143-160, 2000.
- [29] X. Zhang and C.-W. Shu. On maximum-principle-satisfying high order schemes for scalar conservation laws. *Journal of Computational Physics*, 229(9):3091-3120, 2010.
- [30] R.M. Ziff. New solutions to the fragmentation equation. *Journal of Physics A: Mathematical and General*, 24(12):2821-2828, 1991.
- [31] R.M. Ziff and E.D. McGrady. The kinetics of cluster fragmentation and depolymerisation. *Journal of Physics A: Mathematical and General*, 18(15):3027-3037, 1985.